Charge transport properties of Ru-complex molecules: the influence of humidity

Atesci, H.

7. Correlation between ligand structure and charge-transport properties of dinuclear ruthenium complex molecular junctions

In the previous chapters, we have discussed charge transport properties of **2-Ru-N** as a function of humidity, using mononuclear Ru-complexes, i.e. **1-Ru-N** and **1-Ru-Py**, as references. Here, we investigate the effects of subtle changes in the ligand structure on charge transport, as well as electrochemical properties. We do this by comparing **2-Ru-N** to other dinuclear Ru-complexes, i.e. **2-Ru-C** and **2-Ru-N-dec**, thus discretely varying the coupling between the two Ru ions.

7.1 Introduction

In Chapters 4-6, we have investigated humidity-dependent charge transport in **2-Ru-N** molecular junctions in considerable detail. As a reference so far, we have used mononuclear Ru-complexes, i.e. **1-Ru-N** and **1-Ru-Py**, which we view as effectively single-level systems for charge transport. These molecules show negligible rectification at any humidity. Here, we aim to further investigate the interesting properties of dinuclear Ru-based organometallic complexes, and specifically, the relationship between structure and conductance, as a function of humidity. Specifically, we consider the series **2-Ru-N-dec**, **2-Ru-N**, and **2-Ru-C**. To our knowledge, there is insufficient scientific literature that specifically addresses the correlation between ligand structure(*129, 130*) and conductance properties of organometallic complex based molecular junctions under the influence of external trigger, like local humidity.

Here, we report the charge transport behavior of a series of redox-active, conjugated dinuclear ruthenium complexes as a function of ligand structure, discretely varying the coupling between the metal centers. Data are collected in the measurement chamber at low and high values of relative humidity (Fig. 7.1). In addition, we present electrochemical measurements which give independent information on the electrostatic coupling between the Ru centers in the three dinuclear molecules considered.

7.2 Experiment

For the C-AFM measurements, we basically use the same experimental methods as described in Ch. 5 and 6. Likewise, we also use a Au-coated cantilever and 10.5 nN of exerted force on our SAMs. The experiments in our AFM chamber are performed at either low (≈5%) and high humidity (≈65%). The three types of Ru-complexes that are investigated are shown in Fig. 7.1.

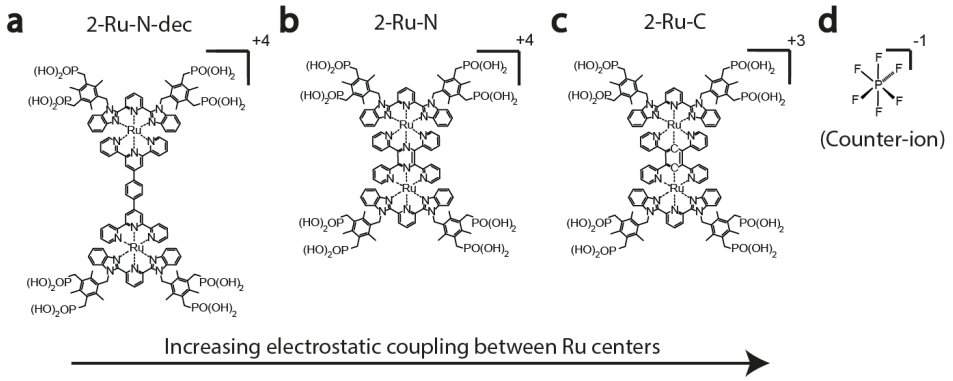

Figure 7.1: The C-AFM tip apex is in contact with a self-assembled monolayer (SAM) on an indium tin oxide substrate. The molecules are of three types, namely **2-Ru-N-dec**, **2-Ru-N**, and **2-Ru-C**, whose symbolic representations we show here. Their corresponding chemical structures are given in (a), (b), and (c) respectively. In all cases, the charged molecules are neutralized by the PF_6^- counter-ion (d).

All three di-nuclear ruthenium complex (**2-Ru-N-dec**, **2-Ru-N**, **2-Ru-C**) molecules contain tetrapodal phosphonic acid anchoring groups, symmetric on both sides. We have characterized all three types of Ru-complex SAMs with cyclic voltammetry to confirm well-formed layers with high surface coverage, as explained in Chapter 3. For convenience, however, we will again show the relevant electrochemical data, see Fig. 7.2.

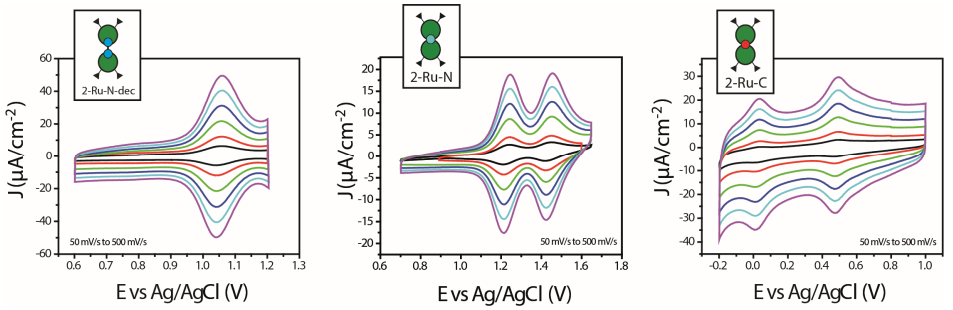

Figure 7.2: Cyclic voltammograms of **2-Ru-N-dec** (a), **2-Ru-N** (b), **2-Ru-C** (c) monolayers measured in 0.1M $HClO_4$ in CH_3CN with scan rates of 50 -500 mVs^{-1} (purple – black) respectively.

Cyclic voltammograms of **2-Ru-N** SAMs (Fig. 7.2b) show two separate reversible redox peaks at +1.21 and +1.42 V. These correspond to the oxidation of Ru(II)–Ru(II) ⇒ Ru(III)–Ru(II) and Ru(III)–Ru(II) ⇒ Ru(III)–Ru(III), respectively. The peak splitting is a measure for the electrostatic coupling of the two Ru-centres in this molecule, which is relatively strong in this case (*131*).

For **2-Ru-C**, the electrochemical data of Nagashima *et al.*(*129, 132*) show that the two redox peaks of **2-Ru-C** are located at -0.40 V and +0.07 V against the Fc^+/Fc reference electrode. Our electrochemical data (in Fig. 7.2c) show that two redox peaks located at +0.02 V and +0.48 V against the Ag/AgCl reference electrode. Now this brings us to the question of in which oxidation state (2+/2+, 2+/3+ or 3+/3+) the Ru atoms of our **2-Ru-C** films are at zero bias. This is hard to determine, because the peak positions in the electrochemical measurements are naturally not at the same potential in the conductance measurements because of the very different experimental conditions (e.g. the presence of liquid electrolyte in the cyclic voltammetry experiment and applied potential is controlled versus a reference electrode).

The larger separation indicates a significantly stronger electrostatic coupling of the two Ru-centres in **2-Ru-C** than in **2-Ru-N**. As the **2-Ru-C** film exhibits relatively low redox potentials for the Ru(II)/Ru(III) pair, it is anticipated that the oxidation states of the **2-Ru-C** SAM can be easily changed by applying a potential(*129, 132*). As discussed before in Chapter 3, the peak separation is indicative of the electrostatic coupling between the Ru centers. By increasing the distance between the Ru centers, the electrostatic coupling between the Ru centers is reduced, moving the peaks closer to each other. In Fig. 7.2a we can see in contrast to both **2-Ru-N**, **2-Ru-C**, that the cyclic voltammetry data of **2-Ru-N-dec** shows only one redox peak, corresponding to a two-electron transfer process (Ru(II)-Ru(III) oxidation), signifying the absence of electrostatic coupling between two ruthenium centers(*129*).

7.3 Results

In Figures 7.3 to 7.5, we present transport measurements on **2-Ru-N-dec**, **2-Ru-N** and **2-Ru-C** junctions at low and high relative humidity, respectively. Results are again shown in the form of logarithmically binned-2D histograms of the absolute current vs. voltage.

Let us start with the molecule with the least electrostatic coupling between Ru centers, **2-Ru-N-dec**. We show the results of the C-AFM measurements in Fig. 7.3. In contrast to **2-Ru-N** in the previous chapters, its |I|-V characteristics are nearly symmetric, with seemingly a slight reduction in RR in humid conditions compared to dry conditions.

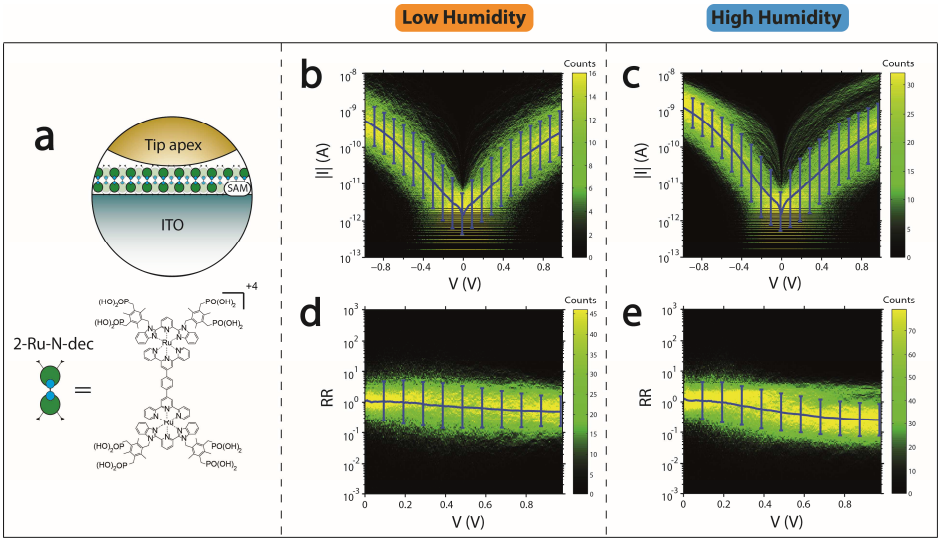

Figure 7.3: Shown in (a) is the schematic representation of the **2-Ru-N-dec** molecular junction. The 2D histogram of logarithmically binned |I|-V characteristics of **2-Ru-N-dec** molecular junctions are shown for (b) low humidity (≈5%) and (c) high humidity (≈65%) conditions. Their corresponding 2D histograms of logarithmically binned RR-V curves are shown for low humidity (d) and high humidity (e). Overlaid in blue is the mean of the Gaussian fits at each bias voltage bin. The error bars follow from the half widths of the fits.

Next, **2-Ru-N** follows with increased electrostatic coupling between Ru centers. We again note in Fig. 7.4 its remarkable switching property as a function of humidity: the RR at 0.9 V changes remarkably from $10^{0.4\pm0.4}$ in dry conditions to $10^{3.0\pm0.6}$ in humid conditions, as we have seen before in Chapters 4-6.

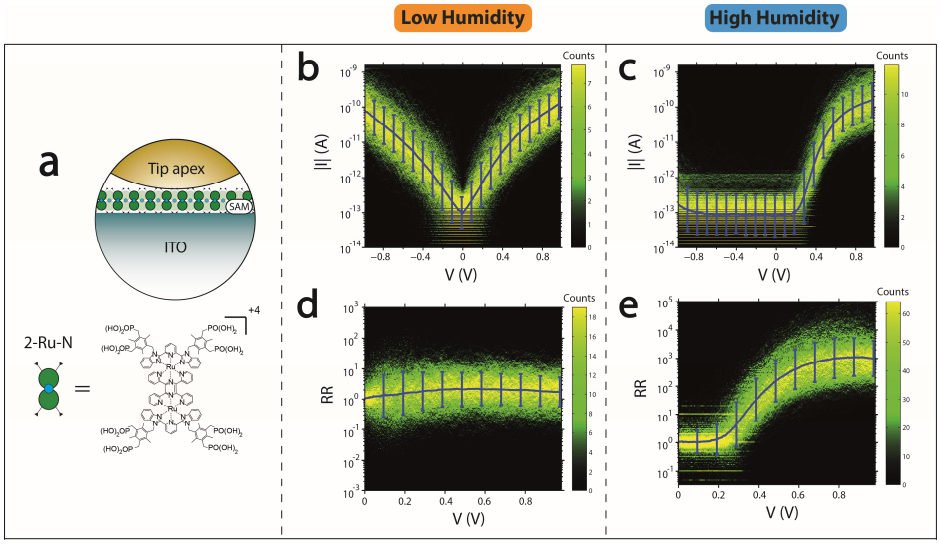

Figure 7.4: Shown in (a) is the schematic representation of the **2-Ru-N** molecular junction. The 2D histogram of logarithmically binned |I|-V characteristics of **2-Ru-N** molecular junctions are shown for (b) low humidity (≈5%) and (c) high humidity (≈65%) conditions. Their corresponding 2D histograms of logarithmically binned RR-V curves are shown for low humidity (d) and high humidity (e). Overlaid in blue is the mean of the Gaussian fits at each bias voltage bin. The error bars follow from the half widths of the fits.

The last molecule on our list, **2-Ru-C**, is similar to **2-Ru-N** structurally, but has a much larger electrostatic coupling between the Ru centers. The results of the conductance measurements are shown in

Fig. 7.5. We can summarize our observations as follows: First, just as for **2-Ru-N-dec** and **2-Ru-N**, **2-Ru-C** exhibits symmetric I-Vs in dry conditions, with perhaps a slight asymmetry towards higher voltages. Second, **2-Ru-C** shows rectification in humid conditions, albeit much less compared to **2-Ru-N**. The RR at 0.9 V is $10^{0.4\pm0.2}$ and in dry conditions it is $10^{-0.1\pm0.2}$. Interestingly, we also notice hysteretic behavior between -1 V and 0 V, when comparing the blue 'trace' curves (where we ramped the voltage from -1 V to +1 V) and the red 'retrace' curves (where we ramped the voltage from +1 V to -1 V).

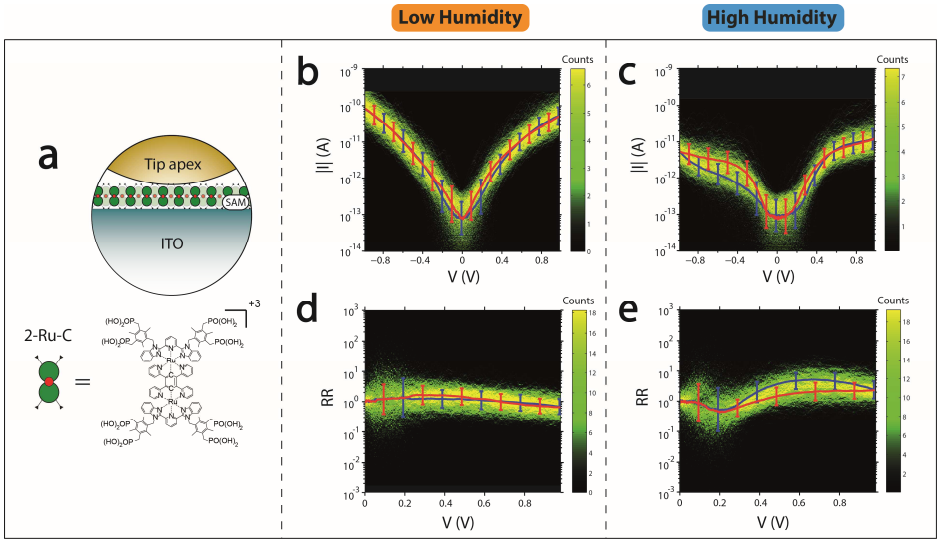

Figure 7.5: Shown in (a) is the schematic representation of the **2-Ru-C** molecular junction. The 2D histogram of logarithmically binned |I|-V characteristics of **2-Ru-C** molecular junctions are shown for (b) low humidity (≈5%) and (c) high humidity (≈65%) conditions. Their corresponding 2D histograms of logarithmically binned RR-V curves are shown for low humidity (d) and high humidity (e). Overlaid in blue and red are the mean of the Gaussian fits at each bias voltage bin for the "trace" (when sweeping the bias voltage from -1V to +1V) and "retrace" (when sweeping the bias voltage from +1V to -1V) measurements, respectively. The error bars follow from the half widths of the fits.

To investigate this further, we have done additional measurements that are extra sensitive, having slow ramp rates (0.01 – 0.03 Hz), on **2-Ru-C** SAMs. We show these in Fig. 7.6. Interestingly, these new data reveal an additional feature in the I-V spectra, namely a hysteretic loop between 0 V and 0.5 V. Thus, **2-Ru-C** shows two hysteretic loops in both negative and positive bias values. It is the only Ru-complex on our list that shows this kind of behavior.

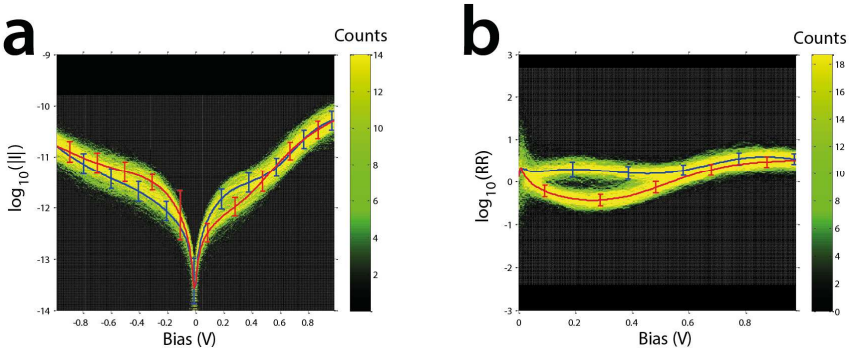

Figure 7.6: (a) The 2D histogram of logarithmically binned |I|-V characteristics of **2-Ru-C** molecular junctions are shown for high humidity (≈65%) conditions. Their corresponding 2D histograms of logarithmically binned RR-V curves are shown in (b). Overlaid in blue and red are the mean of the Gaussian fits at each bias voltage bin for the "trace" (when sweeping the bias voltage from -1V to +1V) and "retrace" (when sweeping the bias voltage from +1V to -1V) measurements, respectively. The error bars follow from the half widths of the fits. The measurements are done with an extra slow bias sweep (0.01 – 0.03 Hz).

We summarize the measurements on all three molecules in Figure 7.7a, where RR(V=0.9V) is plotted for each humidity condition (including ambient: first data point). Also, we show the averaged |I|-V spectra for all three molecules for dry conditions in Fig. 7.7b. This is important for comparing conductance values between the molecules without taking into consideration the effect of water.

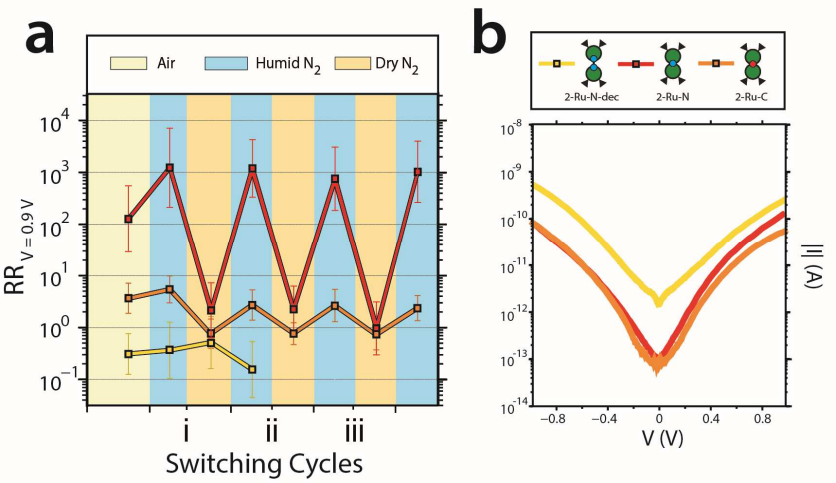

Figure 7.7: (a) RR(V=0.9V) plotted for each consecutive measurement for **2-Ru-N-dec** (yellow line), **2-Ru-N** (red line) and **2-Ru-C** (orange line) with Au tips, as a function of the atmospheric composition. Changing between low (≈5%) and high (≈65%) humidity takes approximately 30 minutes, and measurements for each value of the humidity last 30-60 minutes. (b) The mean values of the Gaussian fits to the absolute current |I| are plotted vs. voltage V for all three molecules (using the same color scheme) in dry conditions.

From Fig. 7.7a we first note that in dry conditions, **2-Ru-N** and **2-Ru-C** have more or less symmetric |I|-V spectra, while **2-Ru-N-dec** is slightly asymmetric. Furthermore, it is only during humid N_2 purging that deviations occur from this state and asymmetries occur, primarily for **2-Ru-N** and **2-Ru-C**. Secondly, we can note over several switching cycles that qualitatively, the same 'switching' behavior for **2-Ru-N** and **2-Ru-C** can be observed. Quantitatively, however, **2-Ru-C** has a significantly smaller response to water compared to **2-Ru-N**. Additionally, **2-Ru-C** exhibits hysteretic effects. And finally, **2-Ru-N-dec** does not show a clear humidity-dependent response in its RR values.

Now, when we compare the current values between the molecules during dry conditions in Fig. 7.7b, we note the relatively high conductance of **2-Ru-N-dec** compared to **2-Ru-N** and **2-Ru-C**. This is intuitively unexpected since the molecular length of **2-Ru-N-dec** is larger (> 0.5 nm) compared to the other two molecules.

7.4 Discussion

The experimental results on the dinuclear Ru complexes contain several surprising elements. Unfortunately, modeling for these molecules is challenging and expensive, due to the complicated nature of these complexes. Hence, time limitations have restricted us from making a complete set of calculations on **2-Ru-N-dec** and **2-Ru-C**, in contrast to the case of **2-Ru-N**. However, we are able to discuss our results in a limited fashion in the light of an elastic tunneling model, with orbital structure calculations based on DFT. In the future, more complex models can be considered.

7.4.1 Ru-complex 2-Ru-N

Let us start with **2-Ru-N**: we have discussed to a large degree its switchable diode-like properties in Ch. 4-6 based on an elastic tunneling model. In summary, when comparing the HOMO and the HOMO-1 distributions of **2-Ru-N** in Fig. 7.8, we note that, approximately, the left hand side is anti-symmetric and the right hand side is symmetric. Adding and subtracting the HOMO and HOMO-1 orbitals will then result in two

LMOs localized around each Ru atom. Water (i.e. simulating humid conditions) breaks the symmetry of the system, causing LMOs to misalign. Thus, a diode-configuration evolves in humid conditions. The **2-Ru-N** model will form the basis to discuss the model for the other molecules.

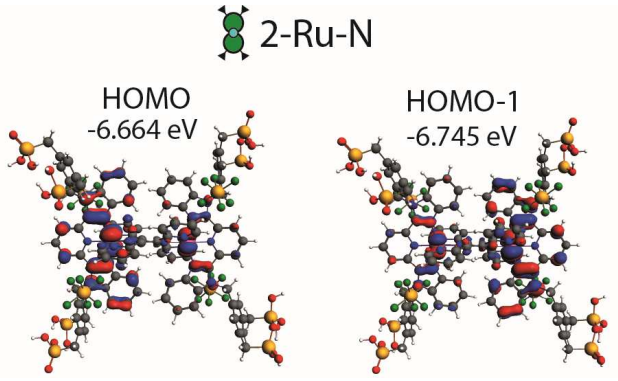

Figure 7.8: Orbital distributions of the HOMO and HOMO-1 for **2-Ru-N**.

7.4.2 Ru-complex 2-Ru-N-dec

As for **2-Ru-N-dec**, we note that in humid conditions, its |I|-V characteristic is relatively symmetric. We have calculated the orbital structures of a variety of levels with DFT and show these in Fig. 7.9.

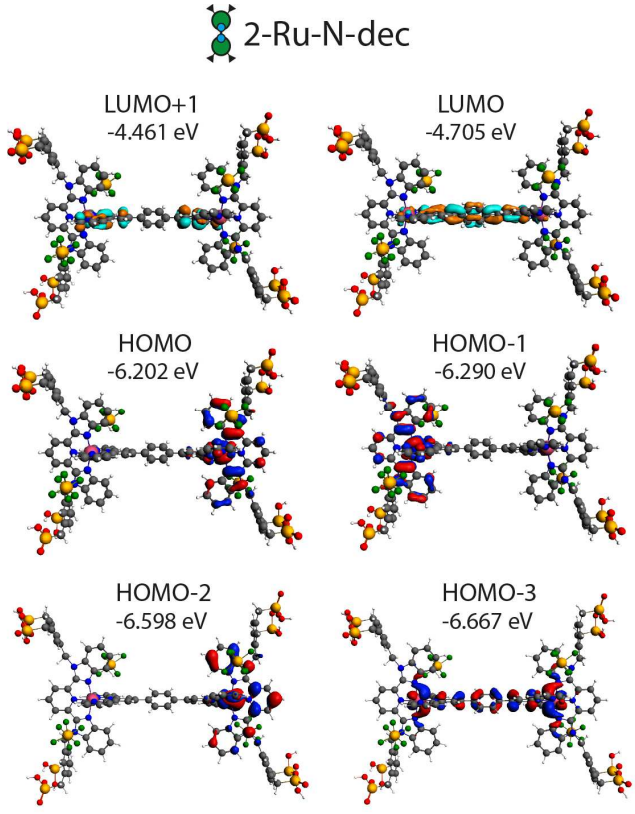

Figure 7.9: Orbital distributions of the LUMO+1, LUMO, HOMO, HOMO-1, HOMO-2 and HOMO-3 for **2-Ru-N-dec**.

We note that **2-Ru-N-dec** too has a distribution of HOMO and HOMO-1 that may be described in terms of two LMOs, just like **2-Ru-N**. This brings us to a logical question: if **2-Ru-N-dec** has a two-site system, then why would it not rectify like **2-Ru-N** during humid conditions?

We hypothesize from the orbital structures that the overlap between the two LMOs must be very small, giving it a relatively small electronic coupling constant τ, due to a relatively large distance between the LMOs. This would translate to a low transmission through the two-site system. In that case, the current may be dominated by other orbitals, nearby in energy, provided that their transmission peaks show considerable broadening. From Fig. 7.9, two candidates arise: the LUMO and the HOMO-3 both of which are delocalized across the entire backbone of the molecular structure. If transport through one of these states is dominant, we would expect a relatively high conductance. Furthermore, as compared to transport through the HOMO and HOMO-1 combinations (LMOs), we are effectively back to a single-level system, behaving much like the mono-nuclear **1-Ru-N** and **1-Ru-Py** complexes. In that case, rectification due to differences in electrode configuration could take place, but the large enhancement of rectification with humidity, as seen in **2-Ru-N**, is not expected. This is qualitatively consistent with our data. To confirm this tentative idea, more detailed calculations are to be performed.

7.4.3 Ru-complex 2-Ru-C

The case of **2-Ru-C** is more complex as two phenomena are observed in Figs. 7.5-7.7. First, whereas **2-Ru-C** shows symmetric I-Vs in dry circumstances, it does exhibit significant rectification in the humid case, similar to **2-Ru-N**. The values found for RR, however, are small compared to those for **2-Ru-N**. Second, for **2-Ru-C** we find hysteretic effects in the IVs, which do not vanish upon making slower voltage sweeps. Hence, they appear to be intrinsic to the system, rather than being related to a trivial RC-time effect (capacitive loading and unloading).

There is more that is special about this molecule. From our electrochemical data in Fig. 7.2, we find that **2-Ru-C** exhibits the strongest electrostatic coupling between the Ru centers of the three molecules considered here. Furthermore, we see that the redox potentials of **2-Ru-C** are considerably lower (close to 0V) than those for **2-Ru-N** when considering the Ag/AgCl reference electrode. Therefore, it is likely that the **2-Ru-C** is either in the +2/+2, +3/+3 or a mixed +2 and +3 oxidation state. It is difficult to verify either of these cases, as we lack sufficient evidence from electrochemistry and DFT calculations to convert this into the voltage scale used in our experiment. Nevertheless, to gain more insight into this system, we performed a limited number of calculations where we investigated the +2/+2 oxidation state of **2-Ru-C**, the results of which are shown in Fig. 7.10.

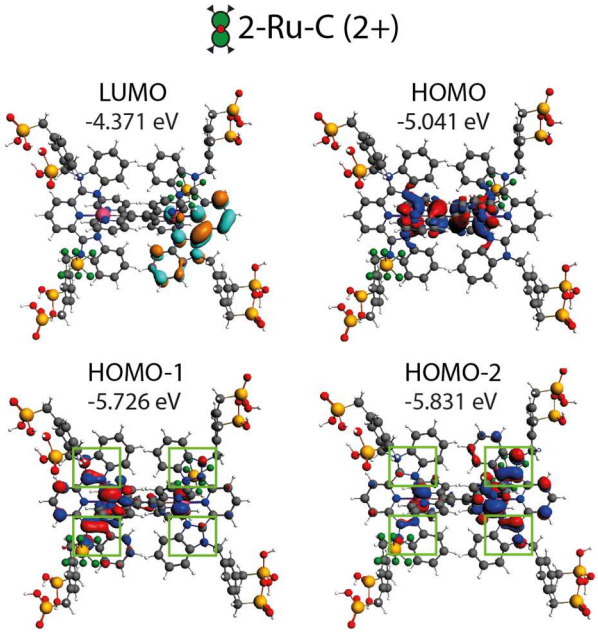

Figure 7.10: Orbital distributions of the LUMO, HOMO, HOMO-1 and HOMO-2, for **2-Ru-C** (2+/2+ oxidation state). For the HOMO-1 and HOMO-2 orbital distributions, green boxes are highlighted over the areas with the intention of comparing the wave function signs between the left and right hand side of the molecule.

For the +2/+2 oxidation state, we note that the LUMO and HOMO orbitals form distinct states that do not show a symmetry or anti-symmetry relation with another state. The HOMO-1 and HOMO-2 states, however, do appear to form a pair. Upon comparing their structure, especially in the highlighted green boxes, we can note that, approximately, the left hand side is symmetric and the right hand side is anti-symmetric. This situation is analogous to the case of HOMO and HOMO-1 in **2-Ru-N** (See Fig. 7.8) so we may expect these orbitals to form two LMOs at each Ru center. Due to insufficient data for the +2/+3 and +3/+3 oxidation states, we can only speculate that a similar two-site system may develop in these states as well.

Nevertheless, from the orbital energies, we can note that the +2/+2 oxidation states of **2-Ru-C** exhibit two orbital states that can be represented by two LMOs located at each Ru center, i.e. they contain a two site system. Also, due to the close proximity of the Ru centers (just like in **2-Ru-N**) and the orbital wavefunction being spread at both halves of the molecule, we speculate that the orbital overlap between the two LMOs (expressed by the coupling constant τ) should be similar to that of **2-Ru-N**, while being higher than that of **2-Ru-N-dec** which only shows the HOMO and HOMO-1 orbital wavefunctions at either half of the molecule.

We have summarized the results of the DFT calculations on the molecular orbitals all dinuclear Ru-complexes in Fig. 7.11. We have also included in red boxes where we suggest a two-site system is likely to be found.

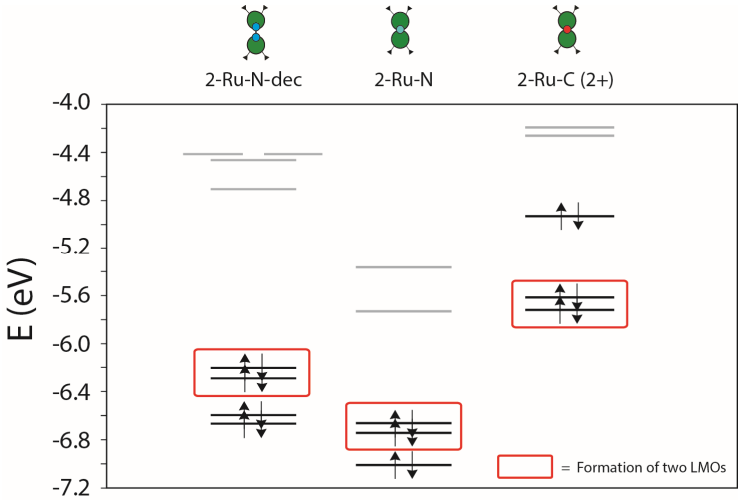

Figure 7.11: Energy diagram of the molecular orbitals of **2-Ru-N-dec**, **2-Ru-N** and **2-Ru-C** (+2 oxidation state). Given in red boxes are the molecular orbitals that can be described by two LMOs in series.

Thus, for **2-Ru-C**, we have a situation where the predominant contribution to the current would be through single level states, due to their proximity to the Fermi levels, with a secondary contribution to the current by the two-site system. Here, we cannot ignore the contribution of the two-site system (which arguably we could in case of **2-Ru-N-dec**), due to the similar electronic coupling between the LMOs, analogous to **2-Ru-N**. Qualitatively, this is inverse to **2-Ru-N**, where the two-site system is closer in proximity to the Fermi levels than the lower-lying single level states that would start significantly contributing to the current at high bias values. Therefore, **2-Ru-C**, would have a lower rectification ratio compared to **2-Ru-N**.

7.4.4 Hysteresis observed in 2-Ru-C

Now we can move on to discussing the hysteretic behavior we observe in **2-Ru-C**. Due to absence of detailed DFT calculations on the +2/+3 and +3/+3 oxidation state (or other supporting data) we will keep our discussion general.

Still, the **2-Ru-C** in any case exhibits relatively low redox potentials and it is anticipated that the oxidation states of the **2-Ru-C** SAM can be easily changed by applying a potential. A change in oxidation state during a bias sweep will then change the electronic structure of the molecule and thus its conductance, which can be observed in the conductance measurement.

Similar observations are also reported by Schwarz *et al.*,(*133*) and Kim *et al.*,(*134*) for ruthenium complexes with relatively small redox potentials. Especially relevant for our case is the explanation for the hysteresis provided by Schwarz *et al.*. They have interpreted the hysteretic behavior observed in the conductance data within a model that incorporates a 'fast channel' and a 'slow channel'. The conductance of the fast channel is governed by a coherent tunneling channel mediated by a delocalized molecular orbital (MO). The slow channel is related to charging of a localized MO. The latter, slow process gives rise to hysteresis. The probability that the localized MO is occupied determines the respective conductance contributions from the two oxidation states at every value of the bias. The model by Schwarz *et al.* may form the basis for a more involved model for explaining our **2-Ru-C** data.

7.5 Conclusion

In conclusion, we have sought to investigate the effects of the ligand structure on the charge transport properties of dinuclear ruthenium complexes **2-Ru-N**, **2-Ru-N-dec** and **2-Ru-C**, for both dry and humid conditions.

We have found that in comparison to the strongly rectifying **2-Ru-N** (with $RR_{0.9V}=10^{3.0\pm0.6}$), the **2-Ru-C** molecule also shows rectification but to a significantly lesser degree in humid conditions (with $RR_{0.9V}=10^{0.4\pm0.2}$). Also, for **2-Ru-C**, hysteretic behavior was observed in humid conditions. The **2-Ru-N-dec** molecule showed a much smaller response to humidity with its I-V spectra being nearly symmetric in both humid and dry conditions.

We have discussed the experimental data in light of DFT calculations on orbital structures and an elastic tunneling model. We have noticed in the orbital structures that the **2-Ru-N** and **2-Ru-N-dec** molecules show a two-site system that would result in a diode configuration in humid conditions by aligning in positive bias and misaligning in negative bias (Ch. 4). The **2-Ru-C** also shows a two-site system in the +2/+2 oxidation state. It is possible that the other oxidation states, namely +2/+3 and +3/+3, also share this property but we have yet to confirm this. Whether the two-site system will actually dominate the current is very much dependent on how they are electronically coupled and whether other orbital levels are closer to the Fermi level: a low electronic coupling would imply that the two-site system does not significantly contribute to the current and would result in an absence of a diode behavior in the conductance measurement. And if other orbital levels are closer to the Fermi level of the electrodes, they would contribute significantly more to the total current, leading to a suppression of rectification ratios. It seems that a correct balance between these factors is necessary to achieve high rectification ratios, as found in **2-Ru-N**.

Furthermore, **2-Ru-C** shows hysteretic behavior (being the only Ru-complex that does so) that may be due to a redox process occurring during bias sweep, especially considering the low redox potentials. However, more detailed calculations are required to come to a better understanding of this phenomenon.